



ALMA MATER STUDIORUM  
UNIVERSITÀ DI BOLOGNA

ARCHIVIO ISTITUZIONALE  
DELLA RICERCA

## Alma Mater Studiorum Università di Bologna Archivio istituzionale della ricerca

Analytical estimation of the key performance points of the tensile force-displacement response of Crescent Shaped Braces

This is the final peer-reviewed author's accepted manuscript (postprint) of the following publication:

*Published Version:*

Palermo M., Laghi V., Gasparini G., Silvestri S., Trombetti T. (2021). Analytical estimation of the key performance points of the tensile force-displacement response of Crescent Shaped Braces. SOIL DYNAMICS AND EARTHQUAKE ENGINEERING, 148, 1-4 [10.1016/j.soildyn.2021.106839].

*Availability:*

This version is available at: <https://hdl.handle.net/11585/828808> since: 2024-03-20

*Published:*

DOI: <http://doi.org/10.1016/j.soildyn.2021.106839>

*Terms of use:*

Some rights reserved. The terms and conditions for the reuse of this version of the manuscript are specified in the publishing policy. For all terms of use and more information see the publisher's website.

This item was downloaded from IRIS Università di Bologna (<https://cris.unibo.it/>).  
When citing, please refer to the published version.

(Article begins on next page)

This is the final peer-reviewed accepted manuscript of:

Michele Palermo, Vittoria Laghi, Giada Gasparini, Stefano Silvestri, Tomaso Trombetti

## Analytical estimation of the key performance points of the tensile force-displacement response of Crescent Shaped Braces

In: Soil Dynamics and Earthquake Engineering, Volume 148, 2021

The final published version is available online at:

<https://doi.org/10.1016/j.soildyn.2021.106839>

### Terms of use:

Some rights reserved. The terms and conditions for the reuse of this version of the manuscript are specified in the publishing policy. For all terms of use and more information see the publisher's website.

*This item was downloaded from IRIS Università di Bologna (<https://cris.unibo.it/>)*

***When citing, please refer to the published version.***

# Analytical estimation of the key performance points of the tensile force-displacement response of Crescent Shaped Braces

Ph.D Michele Palermo<sup>(1)</sup>, Vittoria Laghi<sup>\*(2)</sup>, Ph.D Giada Gasparini<sup>(3)</sup>, Ph.D Stefano Silvestri<sup>(4)</sup>, Ph.D Tomaso Trombetti<sup>(5)</sup>

## Abstract

The technical note investigates the tensile force-displacement response of the hysteretic steel yielding brace known as Crescent Shaped Brace, and characterized by a boomerang-like geometrical shape. The force-displacement curve is governed by three key performance points which correspond to the transition points separating the initial elastic behaviour, the flexural plastic behaviour, the geometrical hardening behaviour and the final axial plastic behaviour. In particular, the influence of the main geometrical parameter of the device, the so-called “lever arm”, on the strongly non-linear force-displacement behavior is analyzed by means of a simplified kinematic model. Based on this, analytical estimations of the key performance points are derived and compared with the numerically simulated force-displacement curves.

## Key words

Crescent Shaped Braces; force-displacement response; geometrical non-linearity; mechanical non-linearity; transition lever arm; key performance points; analytical formulas.

## 1. Introduction

Yielding steel devices are widely used to brace steel structures [1-11]. Among many other solutions presented in the last 40 years, the Crescent Shaped Braces (CSBs) are characterized by a highly non-linear and asymmetric force-displacement  $F-u$  response (as depicted in Figure 1 of [12]) due to their boomerang-like geometrical shape, mainly characterized by the so-called “lever arm”. The mechanical-geometrical coupled nature of the tensile force-displacement response of the CSBs leads to a complex energy dissipation mechanism due to the formation of axial-flexural hinges at the knee-point cross-section [13-17] followed by geometrical hardening and a final axial plastic response.

The first studies on CSBs trace back to the work by Trombetti et al. 2009 [13] which introduced the main feature of a CSB device. Thanks to its original geometrical shape, it is characterized by an initial lateral stiffness which is uncoupled from its lateral yielding strength. This possibility of calibrating the geometrical parameters to obtain selected target responses and the above-mentioned particular  $F-u$  behavior make the CSB suitable as the base component of a lateral-resisting system capable of achieving multiple performance objectives within the Performance Based Seismic Design framework [18].

Analytical studies were carried out to characterize the response up to the first flexural yielding, followed by numerical studies and by a first series of pseudo-static cyclic tests on small scale (1:6) steel CSB devices [16] aimed at characterizing their cyclic non-linear behavior. More recently, a series of experimental quasi-static cyclic tests on a half-scaled single-bay two-storey frame braced with CSBs were also carried out [17].

In this technical note the role of the lever arm in the force-displacement response under monotonic tensile force is investigated considering a simplified kinematic model, from which an analytical estimation of three key performance points is derived. The analytical

estimations of the key performance points allow to predict the ductility and overstrength of the CSB.

## 2. The role of the “transition lever arm” on the F-u response in tension

A CSB made by two straight elements (AC and CB) of equal lengths  $L^*$ , referred to as “symmetric bilinear CSB” is considered (Figure 1a). The angle  $\theta_0$  indicates the initial inclination of each straight segment with respect to the line connecting the two end-points A and B (namely, the horizontal direction in Figure 1a). Point A is fixed, while point B is free to move along the lateral direction ( $u$  indicates the horizontal displacement along the line connecting the two points A and B). The two end supports do not provide any rotational restraint. One of the main geometrical features of the brace is the “initial lever arm”  $d_0$ , namely the vertical distance between the axis connecting A to B (whose length is referred to as  $2L_0$ ) and point C. When the arm  $d_0$  is normalized with respect to the length  $2L_0$ , it is referred to as  $\xi_0=d_0/2L_0$  (subscript  $0$  refers to the undeformed configuration). When subjected to a lateral force  $F$ , the two straight elements of the CSB deform (thick dotted line of Figure 1a) due to the interaction of axial force (compression or tension, depending on the direction of  $F$ ) and bending moment. The angle between the horizontal direction and the chord of one CSB segment in the generic deformed configuration is indicated with  $\theta$  and the corresponding lever arm is indicated with  $d$  (its normalized value is equal to  $\xi=d/2L_0$ ). The vertical displacement of point C is indicated with  $v$ .

The geometrical and mechanical properties of a “symmetric bilinear CSB” are as follows:

- $L^*$  is the length of each straight element;
- $L_0$  is the projection of  $L^*$  in the horizontal plane;
- $\xi_0 = d_0/2L_0$  is the normalized initial lever arm;

- 1 -  $h$ ,  $A$  and  $J$  are the cross-section height, cross-section area and moment of inertia (in-plane), respectively;  
2 -  $i$  is the radius of gyration;  
3 -  $W_e$  is the elastic section modulus of the cross-section;  
4 -  $\beta$  is the shape factor of the cross-section;  
5 -  $E$  is the material Young modulus;  
6 -  $f_y$ ,  $\varepsilon_y$  are the yielding strength and strain;  
7 -  $f_u$ ,  $\varepsilon_u$  are the ultimate strength and strain;  
8 -  $r$  is the hardening ratio.

12 The influence of the geometrical second-order effects on the force-displacement curve can be evaluated by analyzing the kinematic behavior of the equivalent rigid system, e.g. a system made of two rigid straight segments pinned at the knee point C and having the same global geometry as of the CSB. The kinematic behavior of such system is described by a single degree of freedom, for instance the angle  $\theta$  that relates the two displacement components  $u$  and  $v$ :

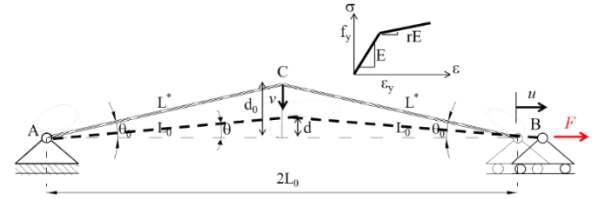
$$\begin{aligned} u &= 2L^* (\cos \theta - \cos \theta_0) \\ v &= L^* (\sin \theta - \sin \theta_0) \end{aligned} \quad (1)$$

22 The incremental displacements  $dv$  and  $du$  are related to  $\xi_0$  by the following analytical expression:

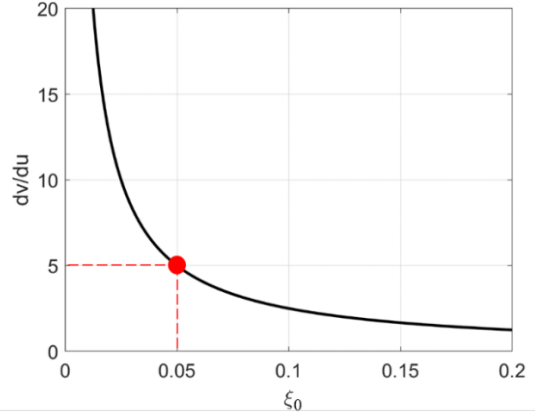
$$\frac{dv}{du}(\theta_0) = \frac{1}{2} \tan^{-1} \theta_0 = \frac{1}{4 \cdot \xi_0} \quad (2)$$

25 Figure 1b displays the trend of  $dv/du$  with respect to the normalized initial arm  $\xi_0$ . The second-order effects cannot be ignored when the incremental displacement  $dv$  becomes much larger than the corresponding incremental displacement  $du$ . This condition occurs when  $dv/du \gg 1.0$ . For practical purposes, a value of  $dv/du = 5$  can be assumed as the “transition” value. From Figure 1b it can be noted that this transition (e.g.  $dv/du = 5$ ) occurs for a lever arm roughly equal to 5%. Such value of the lever arm can be referred to as the “transition lever arm”.

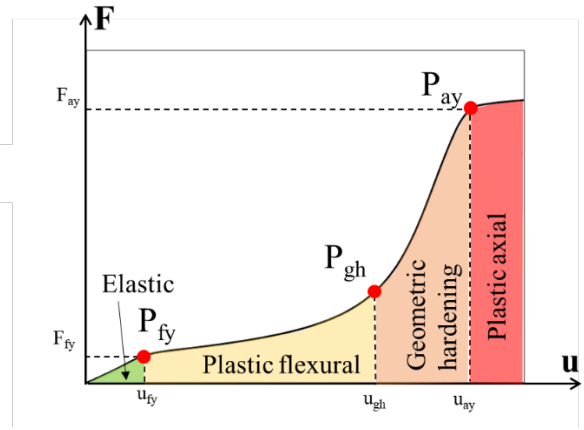
36 The qualitative graphical representations of the  $F-u$  curve of a CSB subjected to tension is shown in Figure 1c. The  $F-u$  curve is made by: (i) a first elastic range (governed mainly by the flexural stiffness) until the first flexural yielding of the knee-point C is achieved (first key performance point  $P_{fy}$ ); (ii) a pseudo-plastic plateau region, governed by plasticity and flexural stiffness, that ends at the transition point (second key performance point  $P_{gh}$ ) with the sudden increase in stiffness due to significant non-linear *geometrical hardening* effects (reduction of the arm  $d$ ) determining the engagement of the axial stiffness; (iii) a geometric hardening region that ends at  $P_{ay}$  (third key performance point) when the brace experiences *axial yielding* while reaching the straight configuration (e.g. the arm  $d$  reduces to zero,  $\xi=0$ ); (iv) a final plastic axial region.



53  
54



55  
56



57  
58

59 **Figure 1:** (a) The “symmetric bilinear” configuration of a CSB subjected to a lateral force  $F$  (adapted from [16]). (b)  $dv/du$  vs  $\xi_0$ . (c) The qualitative  $F-u$  curve of a CSB with indication of the key performance points.

63

### 3. An analytical estimation of the key performance points of CSBs

The initial elastic behavior of the CSB can be described in terms of the initial lateral stiffness and the flexural yielding force (corresponding to the first performance point) as evaluated imposing the equilibrium in the undeformed configuration [12, 16]:

64

65

66

67

68

69

70

71

72

$$F_{fy} = \frac{W_e \cdot f_y}{d_0} \cdot \gamma = \frac{f_y \cdot J}{L_0 \cdot h \cdot \xi_0} \cdot \gamma \quad (3)$$

73

$$u_{fy} = \frac{8}{3} \cdot \frac{f_y \cdot L_0^2 \cdot \xi_0}{E \cdot h \cdot \cos \theta_0} \cdot \gamma \quad (4)$$

74

$$k_{IN} = \frac{3}{8} \cdot \frac{E \cdot J \cdot \cos \theta_0}{L_0^3 \cdot \xi_0^2} \quad (5)$$

$$\gamma = \frac{1}{1 + \frac{h}{2L_0} \cdot \frac{2}{\xi_0} \cdot \left(\frac{i}{h}\right)^2} \quad (6)$$

where  $\gamma$  is a reduction factor ( $\gamma \leq 1.0$ ) depending on the axial force - bending moment interaction.

From Eq. 1, the lateral displacement  $u_{gh}$  (second performance point  $P_{gh}$  corresponding to the  $\xi=5\%$  configuration) results equal to:

$$u_{gh} = 2L_0 \frac{(\cos \theta_{5\%} - \cos \theta_0)}{\cos \theta_0} \quad (7)$$

where  $\theta_{5\%}$  indicates the angle corresponding to the configuration with  $\xi=5\%$ .

The ratio  $u_{gh}/u_{fy}$  can be considered as a measure of the displacement ductility in tension:

$$\mu_t = \frac{3}{4} \frac{E}{f_y} \frac{h}{L_0} \frac{(\cos \theta_{5\%} - \cos \theta_0)}{\xi_0 \cdot \gamma} \quad (8)$$

Eq. 8 clearly highlights that the ductility of the CSB depends on the product of three main factors: a factor related to the material mechanical properties ( $E/f_y$ ), a slenderness parameter ( $h/2L_0$ ) and a function  $f(\xi_0) = (\cos \theta_{5\%} - \cos \theta_0) / (\xi_0 \cdot \gamma)$  dependent on the “distance” between the initial geometrical configuration and the configuration characterized by  $\xi=5\%$ .

The axial yielding force  $F_{ay}$  corresponding to the third performance point  $P_{ay}$  can be evaluated as:

$$F_{ay} = A \cdot f_y \quad (9)$$

The displacement  $u_{ay}$  at point  $P_{ay}$  can be estimated as the sum of the contributions due to the rigid body rotation (Eq. 1) and the elastic deformation  $\varepsilon_y$  (just before yielding point due to axial tension):

$$u_{ay} = \frac{2L_0}{\cos \theta_0} (1 - \cos \theta_0 + \varepsilon_y) \quad (10)$$

The ratio between  $F_{ay}$  and  $F_{fy}$  can be interpreted as an over-strength factor  $\Omega$ :

$$\Omega = \frac{L_0 \cdot h \cdot \xi_0}{i^2 \cdot \gamma} \quad (11)$$

#### 4. Comparisons with the results of non-linear simulations

The level of approximation in the estimation of the key performance points of the  $F-u$  curves according to the proposed analytical equations (Eqs. 1-11) can be appreciated through comparison with the full  $F-u$  response obtained from numerical simulations developed with the Finite Element software SeismoStruct [19]. A CSB device with total horizontal length ( $2L_0$ ) equal to 300 cm and full squared cross-section (10 cm x 10 cm) has been analyzed. Each straight segment of the CSB is modelled with four beam elements using the force-based formulation [20]. Non-linear geometry is approached using the corotational

formulation [21]. Material non-linearity is accounted using an elasto-plastic constitutive model with isotropic hardening (hardening ratio  $r=0.005$ ). Material Young's modulus is set equal to  $E=210000$  MPa and the yielding strength is  $f_y=355$  MPa. The ultimate strain is set equal to  $\varepsilon_u=0.3$ .

Figure 2 compares the analytical piece-wise linear curves (red dashed lines) obtained by simply connecting the three performance points (red dots)  $P_{fy}$ ,  $P_{gh}$  (the force at point  $P_{gh}$  is set equal to  $F_{fy}$ ) and  $P_{ax}$  (as computed according to the analytical formulas derived in the previous section) and the numerical  $F-u$  curves of three CSBs with different  $d_0$  values (30 cm, 45 cm and 60 cm, corresponding to  $\xi_0$  values equal to 10%, 15%, and 20%, respectively). The graphs clearly show that the analytical equations are able to capture the main features of the whole non-linear behavior in tension.

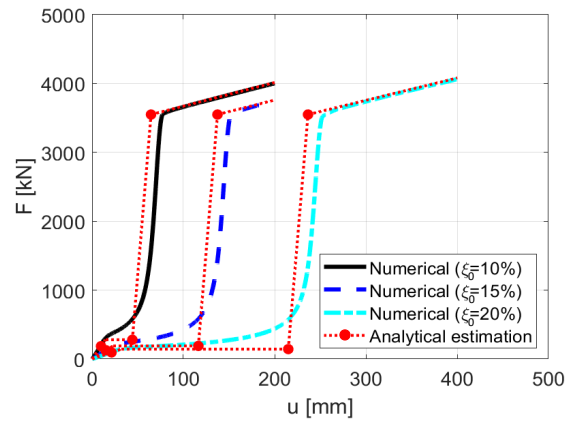


Figure 2: Comparison between numerical  $F-u$  curves and analytical estimation of the key performance points.

It is worth noticing that the shift in the geometrical hardening phase between the analytical and numerical curves is related to the assumed simplified kinematic model (Eq. 1, Figure 1a) which neglects the axial deformation of the CSB. Such approximation appears reasonable for initial lever arms values between 5% and 20%.

It should be noted that the aim of the analytical formulas is not to accurately capture the whole non-linear response, rather to provide practical tools useful for the preliminary design of CSB devices.

#### 5. Conclusions.

This study provides new insights into the non-linear behavior of a steel yielding brace called Crescent Shaped Brace (CSB), which is governed by a strong interaction between geometrical and mechanical non-linearities. The attention has been paid to the tensile post-yielding force-displacement response. It is found that the final geometric hardening behavior (related to the engagement of the axial stiffness due to significant non-linear geometrical effects) experienced under tensile forces after the pseudo-plastic plateau is triggered by a “transition lever arm” corresponding to a normalized value of 5%. This finding indicates that the initial lever arm has to be carefully chosen in order to

1 ensure the required level of ductility under tensile loads. 47  
 2 The force-displacement curve of the CSB in tension is 48  
 3 analytically derived through the definition of three key 49  
 4 performance points, defining different phases of the 50  
 5 CSB behavior: (i) elastic phase, (ii) plastic flexural 51  
 6 phase, (iii) geometric hardening phase and (iv) final 52  
 7 plastic axial phase. The validity of the analytical 53  
 8 estimations is verified through numerical simulations. 54  
 9 The results confirm that the proposed formulas provide 55  
 10 a good level of approximation of the overall force- 56  
 11 displacement behavior of the CSB for preliminary 57  
 12 design purposes. 58  
 59

## 13 References

14  
 15 [1] Skinner RI, Kelly JM, Heine AJ. Hysteretic dampers for 60  
 16 earthquake-resistant structures. *Earthq Eng Struct Dyn* 61  
 17 1974;3:287–96. 62  
 18 [2] Tyler RG. Tapered Steel Energy Dissipators for 63  
 19 Earthquake Resistant Structures. *Bull New Zeal Natl Soc* 64  
 20 *Earthq Eng* 1978;11:282–94. 65  
 21 [3] Whittaker A, Bertero VV, Alonso J, Thompson C. 66  
 22 Earthquake Simulator Testing of Steel Plate Added 67  
 23 Damping and Stiffness Elements. 1989. 68  
 24 <https://doi.org/10.13140/RG.2.1.1455.3207>. 69  
 25 [4] Tsai K-C, Chen H-W, Hong C-P, Su Y-F. Design of Steel 70  
 26 Triangular Plate Energy Absorbers for Seismic-Resistant 71  
 27 Construction. *Earthq Spectra* 1993;9:505–28. 72  
 28 <https://doi.org/10.1193/1.1585727>. 73  
 29 [5] Garivani S, Aghakouchak AA, Shahbeyk S. Numerical and 74  
 30 experimental study of comb-teeth metallic yielding 75  
 31 dampers. *Int J Steel Struct* 2016;16:177–96. 76  
 32 <https://doi.org/10.1007/s13296-016-3014-z>. 77  
 33 [6] Kato S, Kim YB, Nakazawa S, Ohya T. Simulation of the 78  
 34 cyclic behavior of J-shaped steel hysteresis devices and 79  
 35 study on the efficiency for reducing earthquake responses 80  
 36 of space structures. *J Constr Steel Res* 2005. 81  
 37 <https://doi.org/10.1016/j.jcsr.2005.03.006>. 82  
 38 [7] Pujari NN. Optimum Placement of X-Plate Dampers for 83  
 39 Seismic Response Control of Multistoried Buildings. 84  
 40 October 2011;04:481–5. 85  
 41 [8] Baiguera M, Vasdravellis G, Karavasilis TL. Dual seismic- 86  
 42 resistant steel frame with high post-yield stiffness energy- 87  
 43 dissipative braces for residual drift reduction. *J Constr* 88  
 44 *Steel Res* 2016;122:198–212. 89  
 45 [9] Gray MG, Christopoulos C, Packer JA. Cast steel yielding 90  
 46 brace system for concentrically braced frames: concept 91  
 92  
 93

development and experimental validations. *J Struct Eng* 2014;140:4013095.  
 [10] Hsu H-L, Halim H. Improving seismic performance of framed structures with steel curved dampers. *Eng Struct* 2017;130:99–111.  
 [11] Jia L-J, Ge H, Maruyama R, Shinohara K. Development of a novel high-performance all-steel fish-bone shaped buckling-restrained brace. *Eng Struct* 2017;138:105–19. <https://doi.org/10.2174/1874836800903020127>.  
 [12] Palermo M, Silvestri S, Gasparini G, Trombetti T. Crescent shaped braces for the seismic design of building structures. *Mater Struct* 2015;48:1485–502. <https://doi.org/10.1617/s11527-014-0249-z>.  
 [13] Trombetti T, Silvestri S, Gasparini G, Ricci I. Stiffness-Strength-Ductility-Design Approaches for Crescent Shaped Braces. *Open Constr Build Technol J* 2009;3:127–40.  
 [14] Palermo M, Ricci I, Gagliardi S, Silvestri S, Trombetti T, Gasparini G. Multi-performance seismic design through an enhanced first-storey isolation system. *Eng Struct* 2014. <https://doi.org/10.1016/j.engstruct.2013.11.002>.  
 [15] Kammouh O, Silvestri S, Palermo M, Cimellaro GP. Performance-based seismic design of multistory frame structures equipped with crescent-shaped brace. *Struct Control Heal Monit* 2018;25:1–17. <https://doi.org/10.1002/stc.2079>.  
 [16] Palermo M, Pieraccini L, Dib A, Silvestri S, Trombetti T. Experimental tests on Crescent Shaped Braces hysteretic devices. *Eng Struct* 2017;144:185–200. <https://doi.org/10.1016/j.engstruct.2017.04.034>.  
 [17] Mokhtari E, Laghi V, Palermo M, Silvestri S. Quasi-static cyclic tests on a half-scaled two-storey steel frame equipped with Crescent Shaped Braces. *Eng Struct* 2021;232. <https://doi.org/10.1016/j.engstruct.2020.111836>.  
 [18] Bertero RD, Bertero V V. Performance-based seismic engineering: The need for a reliable conceptual comprehensive approach. *Earthq Eng Struct Dyn* 2002;31:627–52. <https://doi.org/10.1002/eqe.146>  
 [19] SoftwareSolutions SEE. SeismoStruct n.d. <http://www.seissoft.com/en/HomePage.aspx>.  
 [20] Spacone E, Ciampi V, Filippou FC. Mixed formulation of nonlinear beam finite element. *Comput Struct* 1996. [https://doi.org/10.1016/0045-7949\(95\)00103-N](https://doi.org/10.1016/0045-7949(95)00103-N).  
 [21] Correia AA, Virtuoso FBE. Nonlinear analysis of space frames. 3rd Eur. Conf. Comput. Mech. Solids, Struct. Coupled Probl. Eng., Lisbon, Portugal: 2006.